COMPUTER TECHNOLOGY IN WELDING

first international conference

LONDON, UK — 3-5 June 1986

Conference Technical Director

W. LUCAS

Preprints

The Welding Institute
Abington Hall Abington Cambridge CB1 6AL

Proceedings of the First International Conference on Computer Technology in Welding

PAPER 13

Computer-aided design of electrodes for manual metal arc welding

L.-E. Svensson, MSc, PhD, B. Gretoft and H.K.D.H. Bhadeshia, BSc, PhD, CEng

SUMMARY

Manual metal arc welding is a complex process involving many variables. In this work we report the development of computer software, based on detailed phase-transformation theory, which allows the theoretical design of primary weld microstructures as a function of chemical composition, welding current, voltage, arc transfer efficiency, interpass temperature, joint geometry and solidification structure. The application of the software is discussed in terms of electrodes for use in the off-shore oil industry.

INTRODUCTION

The microstructure of a weld deposited by an arc welding process depends on variables such as the arc voltage, current, interpass temperature, welding speed, joint geometry, electrode composition, the final deposit composition and the degree of dilution caused by the fusion of the base material. For steels, the problem is complicated further by the numerous transformations which occur during cooling of the weld deposit from the liquidus temperature. The sequence and rate of these transformations is sensitive to the deposit chemical composition, solidification structure and cooling conditions. It is therefore desirable to adopt a fundamental approach towards the development of welding consumables. In this work we demonstrate how a recent model (1) for the prediction of microstructure of weld deposits can be used towards the design welding electrodes, focussing on manual metal arc electrodes for use in the off-shore oil industry. We note that the phase-transformation models (1) used can actually be applied to any low-alloy steel containing Mn, Si, Ni, Cr, Mo, V and C as alloying additions in amy combination, although in this work we concentrate on just Fe-Mn-Ni-Si-C alloys. Furthermore, the electrodes considered are in this instance required to have a strength level in the range 540-560 MPa. The requirement for high toughness limits the C and Si levels in the weld deposit but Ni, due to its intrinsic good effect on toughness (2), can be used in relatively large concentrations while the amount of Mn is limited to < 1 wt.% in order to keep the strength below the maximum specified. The Mn and Ni concentrations studied thus lie approximately within the limits 0.70-1.00Mn and 1.8-3.0Ni, with C and Si fixed at about 0.045 and 0.3 wt.%, respectively.

EXPERIMENTAL

Calculation of the weld microstructure requires the cooling curve of the fusion zone of the weld deposit and stereological information about the columnar austenite grains that develop during solidification (1,3,4). Neither of these can be predicted with sufficient accuracy. The cooling curves are therefore experimentally determined; the γ grain size is sensitive to carbon concentration and to the heat input (1,5,6), but varies less with substitutional alloy content (3). It has also been shown not to depend on inclusion content (4). Since the C concentration is fixed for this study, two experimental welds (using different types of electrodes, as discussed below) with representative concentrations of Mn and Ni, were used to measure the austenite grain parameters. These welds also served to illustrate the fit of experiment with theory.

The welds were deposited by manual metal arc (MMA) welding, the joint geometry being compatible with ISO2560. The welds were deposited, at a rate of 4 mm/s, in the flat position using the stringer bead technique, the parent plate thickness being 20 mm. The welding current and voltage used were 170A and 21V (DC+) respectively, the interpass temperature being 250°C. The welds consisted of some 27 runs with 3 runs per layer. Two different kinds of 4 mm diameter, experimental electrodes (designated types A and B respectively) were used, giving similar deposit compositions (Table 1) but since their coating compositions are different they have significantly different cooling curves, for otherwise identical welding conditions. Weld cooling curves were measured for both types of electrodes and at two welding speeds (4 mm/s and 2 mm/s), by harpooning Pt/Pt-Rh thermocouples at an angle of about 45° to the vertical, into the centre of the weld pool, immediately after the passage of the welding arc. Interpass temperatures were monitored using temperature crayons and thermocouple probes placed on the weld surface.

Table 1 Compositions of experimental weld deposits. The concentrations are in wt.%, except B, O and N which are in ppm by wt. The O concentration is an average of several tests, and in fact varies by $\approx$ 15%.

Weld	C	Si	Mn	Ni	Cr	Mo	Nb	Ti	Al	Cu
1A	0.047	0.27	0.73	2.37	0.03	0.01	0.005	0.011	0.006	0.03
2B	0.045	0.37	1.02	2.29	0.02	0.01	0.008	0.016	0.012	0.02

Weld	Sn	As	Sb	V	Pb	P	S	B	O	N
1A	0.005	0.001	0.001	0.008	0.004	0.016	0.009	$\approx$1	242	96
2B	0.006	0.001	0.001	0.023	0.005	0.007	0.007	$\approx$1	264	64

Optical microscopy was carried out on transverse sections (normal to the welding direction) of the welded samples. The measurements all relate to the as-deposited microstructure of the last run, and were obtained at a magnification of x500. The microstructure was quantified using a Swift point counter with a sample of at least 500 points per weld. Lineal intercept measurements were carried out on a Quantimet 720 image analysing computer, using tracings of the γ grain structure from montages of micrographs taken at x100 magnification. Edge errors arising during measurement were completely avoided by using a guard region, which rejects information from γ grains whose sections lie only partly within the area being analysed. The major axes of the γ grain sections were aligned normal to the scan direction; the mean lineal intercept measurements ($\bar{L}_{tn}$) are thus carried out on transverse sections in a direction normal to the major axes of the grains; it is this parameter which yields information necessary for the calculations that follow (4,7).

THEORY FOR THE PREDICTION OF THE MICROSTRUCTURE

In low-alloy steel welds, solidification begins with the epitaxial nucleation (at the fusion boundary) and cellular growth of δ-ferrite from the melt (8); the δ grains then decompose to a columnar austenite (γ) grain structure whose morphology can be represented as a honeycomb of hexagonal prisms, the side length of each hexagonal prism being 'a' and the length of the prism being 'c' (4,7). The c-axes of these prisms are approximately parallel to the direction of maximum heat flow during solidification; if $\bar{L}_{tn}$ is the mean lineal intercept measured on a transverse section of the weld, in a direction normal to the major axes of the γ grains, then (4)

$$\bar{L}_{tn} = \pi a \cos(30^\circ)/2, \qquad [1]$$

so that 'a' can be determined experimentally. The parameter 'c' is not needed

for the microstructure calculations because c>>a so that any effect due to the ends of the hexagonal prisms can be neglected (1,4). On further cooling, at $T = T_h$, the γ begins to transform, to layers of allotriomorphic ferrite (α) which grow by a diffusional transformation mechanism, at the γ/γ boundaries. As the temperature falls, diffusional growth becomes more difficult and Widmanstätten ferrite (α_w) plates nucleate at the α/γ boundaries and grow into the γ by a displacive transformation mechanism (9), at a rate controlled approximately by the diffusion in C in the γ ahead of the plate tips (10). At the same time, acicular ferrite (α_a) nucleates on inclusions (and also by autocatalytic effects) within the γ grains and grows in the form of thin plates. As the M_s temperature is approached, the small amount of remaining austenite decomposes either into degenerate pearlite and/or mixtures of martensite and retained austenite; because the volume fraction of these phases is relatively small, they are called "microphases".

T_h is determined by using an additive reaction rule (1), the cooling curve and a computed Time-Temperature-Transformation (TTT) diagram for the alloy concerned (11). The TTT diagram consists of two 'C' curves, the upper one giving the time for the isothermal initiation of diffusional transformations such as α and pearlite, while the lower C curve represents the initiation times for displacive transformations such as α_w, α_a and bainite (11). The cross-over point of the two C curves represents the temperature T_1 below which displacive transformations are assumed to be kinetically favoured, so that the growth of α ceases and gives way to α_w and α_a formation. In the temperature range T_h-T_1, the α layers at the $\gamma\gamma$ boundaries are assumed to thicken by a paraequilibrium mechanism, at a rate controlled by the diffusion of carbon in the γ ahead of the moving α/γ interface. During isothermal transformation at a temperature T, the half thickness of each such layer is given by:

$$q = \alpha_1 t^{\frac{1}{2}} \qquad [2]$$

where α_1 is called the one-dimensional parabolic thickening rate constant, obtained by solving (see for example, ref. 12)

$$\{2(x^{\gamma\alpha} - \bar{x})/(x^{\gamma\alpha} - x^{\alpha\gamma})\}\{(\underline{D}/\pi)^{\frac{1}{2}}\}$$

$$= \alpha_1\{\exp[\alpha_1^2/(4\underline{D}/\pi)]\}\{1-\mathrm{erf}[\alpha_1/(2\underline{D}^{\frac{1}{2}})]\} \qquad [3]$$

and t is the time, defined to be zero when q = 0. $x^{\alpha\gamma}$ and $x^{\gamma\alpha}$ are the paraequilibrium carbon concentration of α and of γ respectively, calculated as in Ref.1. The diffusion coefficient D of carbon in γ is a sensitive function of the carbon concentration in austenite (x_γ) and since x_γ varies with distance ahead of the α/γ interface during diffusion-controlled growth, a weighted average diffusion coefficient $\underline{D}$ is used in equation 2, and is defined as

$$\underline{D} = \int_{x^{\gamma\alpha}}^{\bar{x}} D\,dx/(x - x^{\gamma\alpha}) \qquad [4]$$

Since the α grows anisothermally during cooling of the weld deposit, q is actually obtained by numerically integrating the complicated function

$$q = \int_{t=0}^{t=t_1} 0.5\alpha_1\, t^{-0.5}\,dt \qquad [5]$$

where t_1 is the time taken for the weld deposit to cool from T_h to T_1. The volume fraction v_α of α is then derived as a function of a and q:

$$v_\alpha = [4qC_3(a - qC_3)/a^2] \quad [6]$$

where $C_3 = \tan(30^\circ)$. A better fit is obtained by empirically correcting this to give a corrected volume fraction V^α (and this gives a corresponding corrected value of allotriomorph thickness q') where

$$V_\alpha = 2.04v_\alpha + 0.035, \quad [7]$$

the calculated value thus being smaller than the actual value by about a factor of 2, although the correlation between v_α and the actual volume fraction of α is typically found to be 0.95 (1).

At $T = T_1$, α_w formation begins, but the growth rate of α_w in welds is generally so high that growth ceases within a fraction of a second, and α_w formation can therefore be considered to occur isothermally at T_1. However, the volume fraction v_w of Widmanstätten ferrite correlates badly with its lengthening rate (G); impingement with acicular ferrite has to be taken into account. If the time available for unhindered α growth is t_2, then v_w is given by:

$$v_w = 3.34G(a - 2q'C_3)t_2^2/a^2 \quad [8]$$

G is calculated for $T = T_1$, by the method described in (10). In the absence of impingement with α_a, the time available for α_w to grow right across the γ grains is t_3, given by:

$$t_3 = 2(a \sin(60^\circ) - q')/G \quad [9]$$

If t_3 is less than a critical time t_c, then α_w can grow without impingement with acicular ferrite and t_2 in eq. 9 is set to equal t_3. On the other hand, if $t_c < t_3$ than α_w growth is terminated by impingement with a_α, and t_2 is set equal to t_c; t_c is experimentally found to be 0.21s for welds containing inclusions which nucleate acicular ferrite; although t_c is not sensitive to oxygen concentration, it is recognised that it may vary, depending on the ability of inclusions to nucleate acicular ferrite. The microphase volume fraction v_m can also be estimated thermodynamically, so that:

$$v_a = 1 - V_\alpha - v_w - v_m \quad [10]$$

where v_a is the volume fraction of α_a. It is usual to include the microphases in the v_w and v_a measurements, since v_m is generally small; hence, microphases are not measured or calculated separately in this work.

Cooling rates associated with arc welding are non-equilibrium and this inevitably leads to solute segregation during solidification. The biggest effect of such segregation is to alter T_h (7); if solidification occurs with δ as the primary phase, then the partition coefficients k_i (where i is the subscript identifying an alloy element) which give the ratio of the mole fraction of i in δ to that in liquid is given at a temperature T by:

$$k_i = \exp\{\Delta^\circ G_i/(RT)\} \quad [11]$$

where $\Delta^\circ G_i$ is the Gibbs-free energy change per mole in transforming the pure i from δ to liquid, and R is the universal gas constant. Due to the high cooling rates during welding, it is assumed that the segregation arising during solidification is not influenced by subsequent diffusion during cooling from the liquidus. The composition of regions which contain the lowest substitutional content is

then given by $k_i\bar{x}_i$ where $\bar{x}_i$ is the average concentration of i and T is set to the melting point in eq. 11, assumed to be 1520°C. Carbon is assumed uniform everywhere since its activity gradients should rapidly be eliminated by diffusion during cooling. It follows that the compositions of the solute-depleted regions can be calculated, and these are the regions which enhance ferrite nucleation. New TTT curves calculated for these solute-depleted regions can then be used to obtain better estimates of T_h. It has been shown (7) that this procedure works well in calculating the microstructure of welds.

RESULTS

Experimental welds

Cooling curves obtained from welds using types A and B electrodes, are presented in Fig. 1; such curves can be rationalised in terms of equation:

$$dT/dt = (C_1/Q\eta)(T-T_i)^{C_2} \qquad [12]$$

where dT/dt is the magnitude of the cooling rate (°C/s) over the range 800-400°C, T_i is the interpass temperature, Q is the nominal electrical energy heat input (J/m), η is the arc transfer efficiency (0.775) and C_1 and C_2 are constants obtained by fitting eq. 10 to experimental data. In eq. 10, dT/dt in the fusion zone, is independent of position. The relevant constants for the curves presented in Fig. 1 are given in Table 2. The details of the microstuctures of welds 1 and 2 (compositions in Table 1) are presented in Table 3. Representative microstructures of welds 1A and 2B are illustrated in Fig. 2.

Table 2 Analysis of cooling curves presented in Fig. 1. R is the linear regressions correlation coefficient for the plot of $\ln\{(dT/dt)/Q\eta\}$ versus $\ln\{T-T_i\}$, with Q in J/m and dT/dt in °C/s. T_1 and T_2 are the statistical 't' values for the regression constant ($\ln C_1$) and the regression coefficient (C_2) respectively.

Electrode type	C_1	C_2	R	T_1	T_2
A	592.3	1.679	0.997	25.2	39.1
B	1869.0	1.499	0.974	11.6	13.6

Table 3 Microstructure and properties of welds 1,2, which were deposited at a speed of 4 mm/s. Electrode types are indicated by the letters A and B. The lineal intercepts are a mean of 200 measurements, with a standard error of only 2.5 μm. The 95% confidence limits in the measured volume fractions are at most ± 0.045. Charpy results are from an average of 5 tests.

Actual Results	Weld 1A	Weld 2B
$\bar{L}_{tn}$	73	60
v_α	0.31	0.21
v_w	0.27	0.15
v_a	0.42	0.64
UTS, MPa	555	605
Charpy J -50°C, -70°C	156, 109	153, 127
C.O.D., -10°C, mm	0.90-1.22	

Calculated Results	Weld 1A	Weld 2B
V_α	0.34	0.36
V_w	0.18	0.15
V_a	0.48	0.49
q', μm	8.74	7.71
T_h-T_l, °C	722-600	700-600
t, seconds	5.9	4.7
M_s, °C	465	456
G at T_1, μm/s	77.8	53.7
t_2, seconds	0.211	0.211

(Table 3, continued)

Theoretical design of Fe-Mn-Si-Ni-C electrodes

The microstructures of the fusion zones of a series of hypothetical Fe-Mn-Si-Ni-C weld deposits (Table 4) were calculated for both electrode types. The relevant cooling curves were calculated using eq. 10 and the data of Table 2. $\bar{L}_{tn}$ types A and B electrodes is taken to be 73 and 60 μm respectively (Table 3), irrespective of Ni concentration or welding speed. For types A and B electrodes deposited at 2 mm/s, additional calculations were done with $\bar{L}_{tn}$ taken to be 87 and 74 μm respectively, since $\bar{L}_{tn}$ is known to increase by 16 μm for every 1 kJ/mm increase in electrical energy heat-input per mm(3). Solidification is assumed to occur with δ as the primary phase, and at the melting point (assumed to be 1520°C) the partition coefficients for Si, Mn and Ni were calculated to be 0.72, 0.75 and 0.46 respectively, so that the compositions of the solute-depleted regions of any weld can be calculated. The results are presented in Fig. 3, and additional data in Table 5.

Table 4 Chemical compositions (wt.%) of alloys used in the theoretical study

Weld	C	Si	Mn	Ni
3	0.045	0.30	0.70	1.80
4	0.045	0.30	0.70	2.40
5	0.045	0.30	0.70	3.00
6	0.045	0.30	1.00	1.80
7	0.045	0.30	1.00	2.40
8	0.045	0.30	1.00	3.00

Discussion

Consistent with earlier work, the experimental results (Table 3) show that the model can be used to estimate quantitatively, the microstructure of Fe-Mn-Si-Ni-C low-alloy steel weld deposits. The data presented in Tables 2 and 5 indicate that the transformation to α finishes in a few seconds, while that to Widmanstätten ferrite finishes in a fraction of a second. Furthermore, for all the welds studied, the growth of Widmanstätten ferrite is limited by impingement with acicular ferrite ($t_1 = t_c$). The calculations presented in Fig. 3 show that the microstructure is more sensitive to Ni at the lower Mn concentration of 0.7 wt.%; the difference between the low and high Mn welds becomes smaller as Ni increases.

The effect of heat input on microstructure is more complex. If γ grain size is assumed to be unaltered by the welding speed, then the welds deposited at 2 mm/s

Table 5 Ancillary calculated data. The weld identifications are as in Table 4, but have the additional letters A and B, which refer to the electrode type, and hence to the weld cooling conditions. V is the welding speed in mm/s.

Weld	V,mm/s	q′μm	T_h-T_l,°C	t, s	δ mm/s	t_2, s
3A	2	16.4	761-600	14.6	133.3	0.211
4A	2	12.3	741-600	13.2	88.5	0.211
5A	2	9.5	721-600	11.8	52.9	0.211
6A	2	13.5	742-600	13.3	84.4	0.211
7A	2	10.6	720-600	11.7	50.5	0.211
8A	2	9.2	698-580	12.6	47.4	0.211
3A	4	11.5	748-600	6.9	133.3	0.211
4A	4	9.1	725-600	6.0	88.5	0.211
5A	4	7.4	701-600	5.1	52.9	0.211
6A	4	9.7	724-600	6.0	84.4	0.211
7A	4	7.8	698-600	5.0	50.5	0.211
8A	4	6.8	667-580	4.9	47.4	0.211
3B	2	16.2	761-600	13.7	133.3	0.211
4B	2	12.0	740-600	12.3	88.5	0.211
5B	2	9.2	720-600	10.9	52.9	0.211
6B	2	13.2	741-600	12.4	84.4	0.211
7B	2	10.2	719-600	10.8	50.5	0.211
8B	2	8.9	696-580	11.5	47.4	0.211
3B	4	11.2	747-600	6.4	133.3	0.211
4B	4	8.7	724-600	5.6	88.5	0.211
5B	4	7.1	700-600	4.7	52.9	0.211
6B	4	9.3	723-600	5.6	84.4	0.211
7B	4	7.4	696-600	4.5	50.5	0.211
8B	4	6.4	664-580	4.4	47.4	0.211

(Fig. 3) all have lower acicular ferrite contents when compared with those deposited at 4 mm/s. On the other hand, if the γ grain size is realistically assumed to increase due to the extra heat input resulting from the lower welding speed, then the microstructures for the welds deposited at the two welding speeds are very similar, although it is notable from Table 3 that in either case, the q′ values are always higher for the welds deposited at lower speeds; this may have an effect on toughness.

For fixed welding conditions, type A electrodes lead to slower weld cooling rates and higher γ grain sizes; the latter effect dominates and so the acicular ferrite content of type A electrodes is generally higher, but this again hides the fact that the q′ values for type A electrodes are always higher than corresponding values for type B electrodes.

CONCLUSIONS

Phase transformations theory has been used to develop a computer model for the systematic study of the primary weld microstructure as a function of chemical composition and welding conditions. The model provides clear guidance towards the design of consumables for manual metal arc welding.

ACKNOWLEDGEMENTS

The authors are grateful to ESAB AB (Sweden) for financial support and to Professor Hull for the provision of laboratory facilities at the University of Cambridge.

REFERENCES

1. Bhadeshia H K D H, Svensson L-E and Gretoft B: 'A Model for the development of microstructure in low-alloy steel weld deposits'. Acta Metallurgica 1985 33 1271-1283.

2. Leslie W C: 'The physical metallurgy of steels'. McGraw-Hill pub., U.S.A., 1982, 123-124.

3. Svensson L-E, Gretoft B, Bhadeshia H K D H: 'An analysis of cooling curves from the fusion zone of steel weld deposits'. Scandanavian J. of Metallurgy 1986, in press.

4. Bhadeshia H K D H, Svensson L-E and Gretoft B: 'The austenite grain structure of low-alloy steel weld deposits'. J. of Materials Science 1986, in press .

5. Evans G M: 'Effect of C on the microstructure and properties of C-Mn all-weld deposits'. International Welding Institute Document II-A-546-1981.

6. Evans G M: 'Effect of heat-input on the microstructure and properties of C-Mn all-weld metal deposits'. International Welding Institute Document II-490-1979.

7. Gretoft B, Bhadeshia H K D H and Svensson L-E: 'Development of microstructure in the fusion zone of steel weld deposits'. Acta Stereologica 1986, in press.

8. Davies G J and Garland J G: 'Solidification of Welds, International Metall. Rev. 1975 20 83-120.

9. Bhadeshia H K D H: 'Rationalisation of shear transformations in steels', Acta Metall. 1981 29 1117-1130.

10. Bhadeshia H K D H: 'Critical Assessment: Diffusion-controlled growth of ferrite plates in plain-carbon steels, Mat. Sci. and Tech. 1985 1 497-504.

11. Bhadeshia H K D H: 'Thermodynamic analysis of isothermal transformation diagrams', Met. Sci. 1982 16 159-165.

12. Bhadeshia H K D H: 'Diffusional formation of ferrite in iron and its alloys', Prog. in Mat. Sci. 1985 29 321-386.

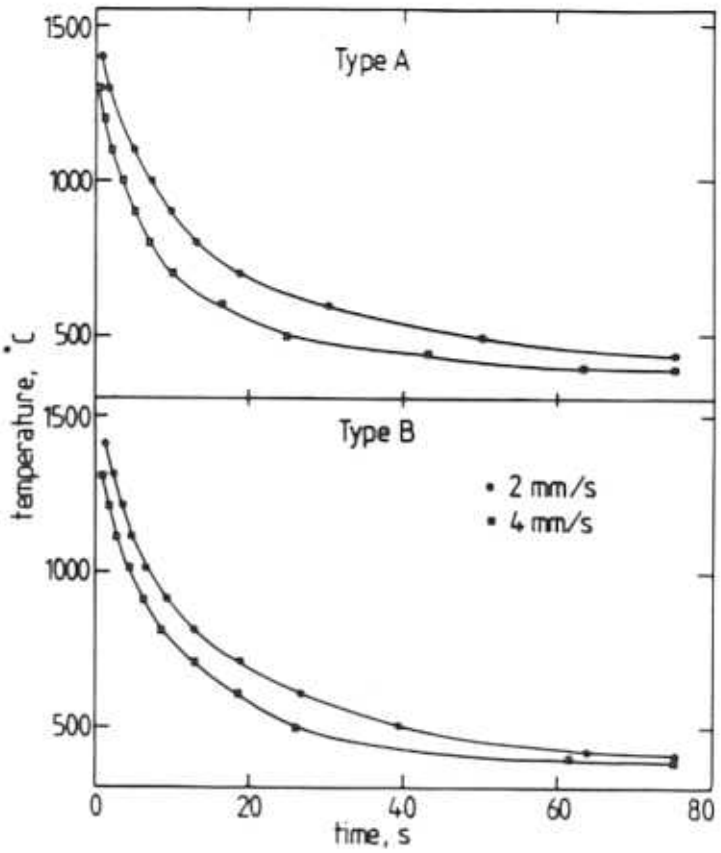

1 Experimentally-measured cooling curves.

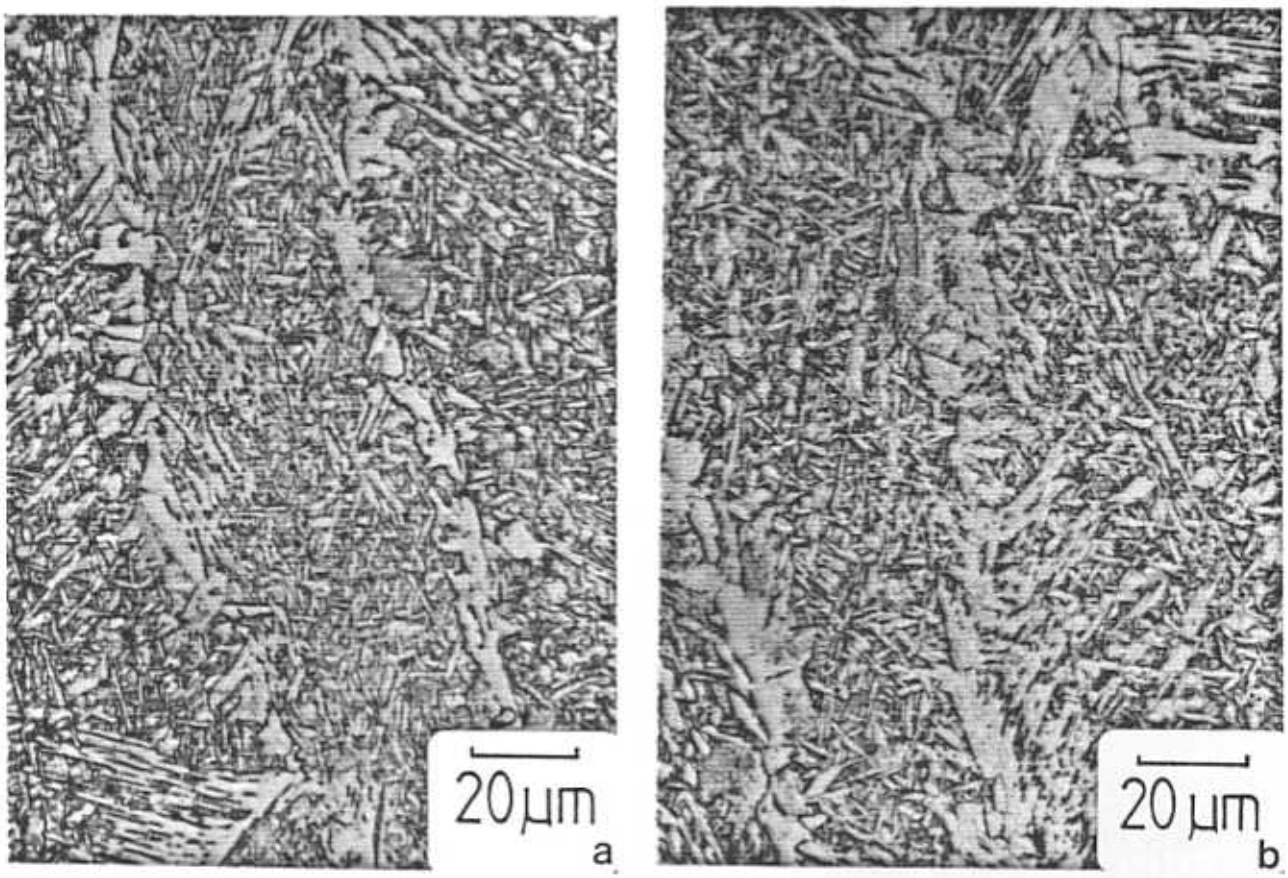

2 Optical Micrographs of the primary microstructure: a) Weld 1A; b) Weld 2B.

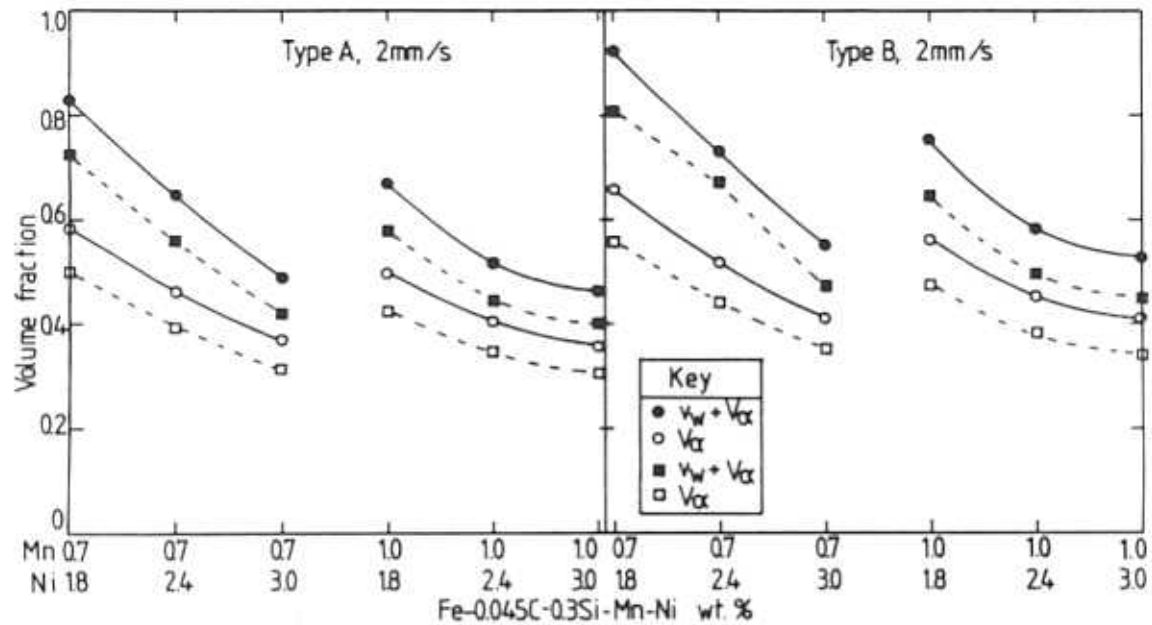

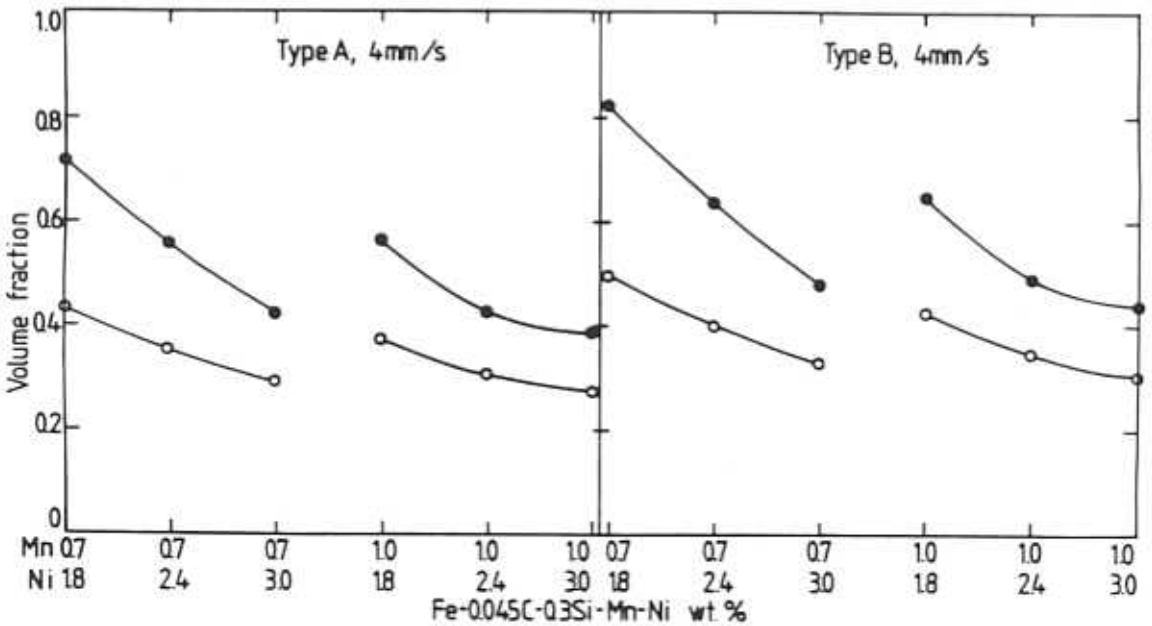

3 Calculated microstructure of Fe-Mn-Si-Ni-C welds. The continuous lines refer to calculations done assuming 2a = 73 and 60 μm for electrodes of type A and B respectively, while the dashed lines assume 2a = 87 and 74 μm for electrode types A and B respectively: a) Welds deposited at 2 mm/s; b) Welds deposited at 4 mm/s.